

Assessment of High-resolution Local Emissions and Land-use in Air Quality Forecasting at an Urban, Coastal, Desert Environment

Christos Fountoukis*, Yasir Mohieldeen, Luis Pomares†, Ivan Gladich, Azhar Siddique, Adam Skillern, Mohammed A. Ayoub

Qatar Environment and Energy Research Institute, Hamad Bin Khalifa University, Qatar Foundation, Education City, 34110 Doha, Qatar

ABSTRACT

Fine particulate matter, ozone and nitrogen oxides are forecasted using a three-dimensional atmospheric meteorology-chemistry model (WRF-Chem) and a triple-nesting configuration over the Middle East and the Arabian Peninsula focusing on the hot desert climate of Qatar. We analyze the impact of a local anthropogenic emission inventory (EI) on model predictions, compared to the most commonly used EDGAR global emissions. The model's forecast accuracy was assessed against measurement data from five ground air quality monitoring stations in the greater metropolitan area of Doha over a one-month period. The footprint of the Doha metropolitan area on the geographical distribution of the anthropogenic emissions is much more realistically represented in the new version of emissions, which includes major differences in the magnitude of emission rates, locally, compared to the base case. The use of the local emissions allowed for a significant improvement in the representation of air quality levels in the city. The overall forecast error decreased from -51% to 8% for PM_{2.5} and from -88% to 20% for NO_x while a significant improvement was observed in the diurnal profile of predicted ozone. The ability of the model to forecast the air quality health index in this urban, coastal, hot desert climate is encouraging for future applications of this modeling platform as an early warning system (EWS).

Keywords: WRF-Chem, Arabian desert, PM_{2.5}, EDGAR emissions

1 INTRODUCTION

Increased levels of air pollution are a major health concern in urban environments worldwide. In fast growing cities of the Middle East, air quality is often negatively affected by increased concentrations of ambient particulate matter, originating from various sources (desert dust, construction activities, resuspended road dust, diesel engines, secondary formation) or ozone which forms photo-chemically through a chain of chemical reactions involving nitrogen oxides and volatile organic compounds emitted mainly from traffic and industrial activities. In the Arabian Peninsula in particular, intense urbanization and industrial activity over the last decades in some countries necessitates efficient air quality management plans for major metropolitan areas where more than 80% of the country's population is currently living. In order to mitigate the negative health effects induced by poor air quality, abatement strategies (Font and Fuller, 2016; Bel and Joseph, 2015) need to tackle both air pollution episodic days as well as elevated background atmospheric pollution levels throughout the year.

A comprehensive air quality management plan requires the use of both modeling and field measurement studies among others. For air quality modeling, the most advanced tool that is used in the design of pollution control strategies is a eulerian three-dimensional chemistry-transport model (CTM) with online-coupled meteorology (Longo *et al.*, 2013; Fast *et al.*, 2006). The application of CTMs for air quality studies is often challenging when the region of interest is

OPEN ACCESS

Received: January 2, 2022

Revised: April 17, 2022

Accepted: April 18, 2022

* Corresponding Author:

cfountoukis@hbku.edu.qa


† Now at Dubai Electricity and Water Authority's Research and Development Centre, UAE

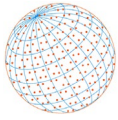
Publisher:

Taiwan Association for Aerosol Research

ISSN: 1680-8584 print

ISSN: 2071-1409 online

 **Copyright:** The Author(s). This is an open access article distributed under the terms of the [Creative Commons Attribution License \(CC BY 4.0\)](https://creativecommons.org/licenses/by/4.0/), which permits unrestricted use, distribution, and reproduction in any medium, provided the original author and source are cited.



a complex environment with various sources of pollution and a strong influence of variable weather conditions. Known components of a CTM that contribute to prediction errors are emissions, parameterizations describing physicochemical atmospheric processes, boundary conditions, terrain characteristics and meteorology. The most significant contributor of model errors is often the emissions input used. Both anthropogenic and biogenic emissions of reactive gases and aerosols (including aerosol precursors) can substantially change the atmospheric composition of an urban center in a rapid rate throughout the day. Accurate quantification of emission rates of pollutants within emission inventories (EIs) is of fundamental importance for a successful implementation of a CTM which uses emission rates and emission time series as a key model input.

At a continental/regional scale the most established emission inventories that have been used within CTMs include the EDGAR inventory (Emission Database for Global Atmospheric Research, <http://www.mnp.nl/edgar/introduction>), the RETRO (REanalysis of the TROpospheric chemical composition, <http://retro.enes.org>) inventory and the recent CEDS (Community Emission Data System) global emission inventory (Hoesly *et al.*, 2018). EDGAR has been widely used by policy makers as it is considered unique in its inclusion of more than 20 years of historical emission data for all countries of the world. EDGAR uses scientific data and international statistics to calculate emission data in a common and consistent way for all countries. However, at a country-scale, deficiencies in these emissions often occur and are significant especially for emerging, fast-growing countries as well as for countries that do not report air pollution measurements consistently. In the Arabian Peninsula due to a scarcity of spatially distributed national emission inventories, EDGAR information alone may be outdated or unreliable when constructing emission input for a CTM application.

There have been limited air quality CTM studies in the Arabian Peninsula so far, most of which largely focused on dust storms and the application of an appropriate dust emission source function for the region (Anisimov *et al.*, 2017; Kalenderski *et al.*, 2013; Jish Prakash *et al.*, 2015; Fountoukis *et al.*, 2020, 2016; Kontos *et al.*, 2018; Karagulian *et al.*, 2019; Parajuli *et al.*, 2019). Much less attention has been given to anthropogenic emissions and their impact on the air quality of urban areas of the Arabian Peninsula (Ukhov *et al.*, 2020; Roshan *et al.*, 2019). The choice of the right emission inventory for this region is not straightforward. Global anthropogenic emission inventories like EDGAR, although widely used, have low spatial resolution that often results in producing spatially smooth and thus locally unrealistic results. On the other hand, the use of EDGAR's database total emission fluxes for CTM at a regional scale provides consistency with regard to the methodology used to construct emissions across all countries and gives confidence in the modeling of transboundary pollution conditions.

In this work, we apply the WRF-Chem (Fast *et al.*, 2006; Grell *et al.*, 2005) model over the Arabian Peninsula in forecasting mode with a focus on the metropolitan area of Doha, Qatar. Based on EDGAR total emission fluxes we construct a local emission inventory using updated high-resolution (250 m × 250 m) land-use information. The goal of this work is to evaluate the impact of a local emission inventory compared to the base case EDGAR on predicting main air pollutant concentrations in an urban environment where local measurement data are available for model evaluation. The methodology to construct the local EI in this study could be used as a prototype for future forecasting WRF-Chem applications that could benefit from improved EDGAR emissions in this region.

2 METHODS

2.1 Model Application

In the arid urban environment of Doha, Qatar, numerous physical and chemical atmospheric processes occur simultaneously, due to various factors such as intense sunlight/photochemistry throughout the year, sea-breeze circulation, strong primary emission fluxes mostly from traffic, construction and industrial activities, the influence of desert dust, transboundary pollution and others. This requires the use of a comprehensive numerical chemical transport model such as the three dimensional meteorology-chemistry model WRF-Chem (Weather Research Forecasting with Chemistry (Fast *et al.*, 2006; Grell *et al.*, 2005). We use the 4.2 version deployed over the Middle Eastern region with an enhanced grid resolution over the state of Qatar (Fig. 1).

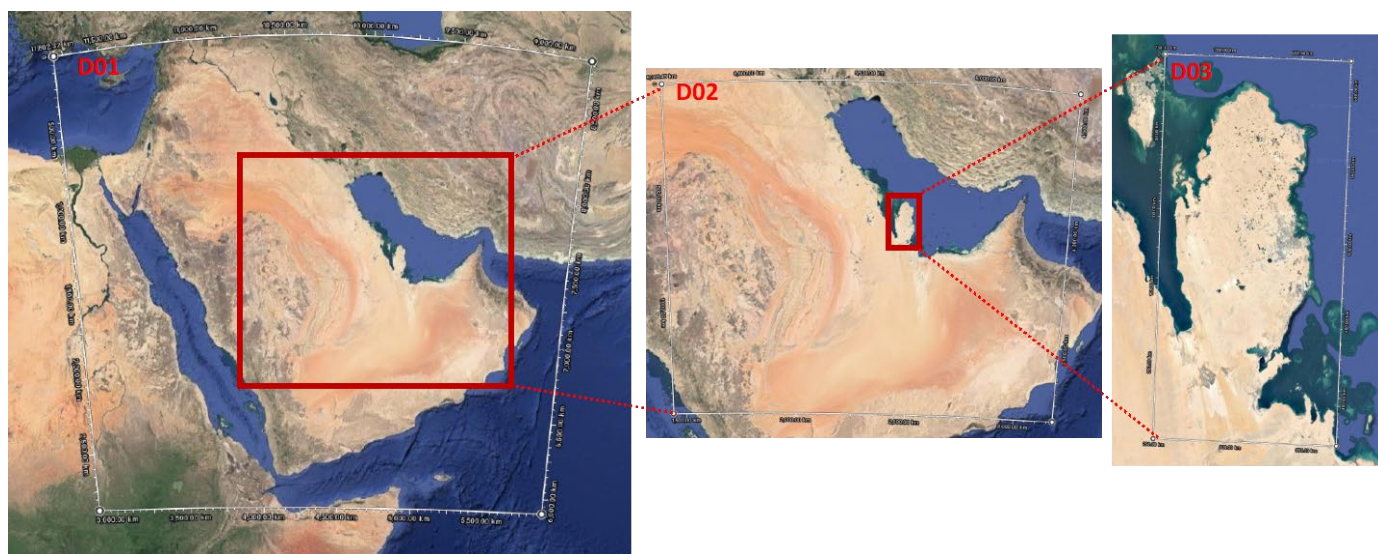
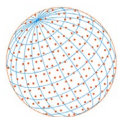
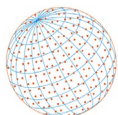


Fig. 1. WRF-Chem configuration of three modeling domains at different grid resolutions over the Middle East region; (left panel): 10.3°–36.1° latitude, 29.5°–63.3° longitude, (50 km × 50 km), (middle panel): 17.2°–30.6° latitude, 40.6°–58.8° longitude, (10 km × 10 km), and (right panel): 24.1°–26.4° latitude, 50.6°–51.9° longitude, (2 km × 2 km).

Lambert map projection was used in all simulations. The parent domain is resolved in a 50 km × 50 km grid while the intermediate nested domain used a 10 km × 10 km resolution over the Arabian desert. The third domain was configured over Qatar where our continuous air quality monitoring stations are located and was resolved at 2 km × 2 km. Twenty eight vertical layers were used in all three computational domains extending from the surface to approximately 20 km. Our selected model configuration is carefully chosen to allow WRF-Chem for a computationally efficient modeling setup capable of spanning large areas in which regional transport of pollutants is important (e.g., frequent dust storms often originating from the greater Middle Eastern region), while providing fine resolution in select areas (e.g., Qatar) to address small-scale features (e.g., high-res emissions). Static geographical data along with dynamic meteorological data generated by the Global Forecast System (GFS) were used to initialize the model. The physics part of the model application includes the Lin microphysics scheme (Chen and Sun, 2002), the Grell 3D cumulus parameterization (Grell and Devenyi, 2002), the Goddard shortwave radiation scheme, the Rapid Radiative Transfer Model longwave radiation scheme (Mlawer *et al.*, 1997), the 5-layer thermal diffusion land surface model, the revised MM5 Monin-Obukhov surface layer scheme and the Yonsei University boundary layer scheme (Hong *et al.*, 2006). For the planetary boundary layer (PBL) parameterization choice, a sensitivity study was conducted to identify the most representative PBL scheme for the atmospheric condition in the Middle East (Fountoukis *et al.*, 2018). The RACM (Regional Atmospheric Chemistry Mechanism) chemistry scheme is utilized (Stockwell *et al.*, 1997; Geiger *et al.*, 2003) coupled with the Georgia Institute of Technology-Goddard Global Ozone Chemistry Aerosol Radiation and Transport (GOCART) aerosol module (Ginoux *et al.*, 2001).

2.2 High-resolution Emissions and Land-use Data

For the base case simulations we use the latest version of EDGAR emissions; namely the HTAP_V2 (Hemispheric Transport of Air Pollution emissions – version 2; <http://www.htap.org/>) anthropogenic emissions, which include black carbon (BC) and organic carbon (OC), particulate matter (PM₁₀ and PM_{2.5}), sulfur dioxide (SO₂), ammonia (NH₃), nitrogen oxides (NO_x), methane (CH₄), carbon monoxide (CO) and non-methane volatile organic compounds (NMVOCs). These emissions are provided for several source sectors: transport, energy, industry, agriculture and residential sector in 0.1° × 0.1° or 0.5° × 0.5° grid maps depending on the species. A grid-mapping program has been used to map the global anthropogenic emissions data to Qatar as well as the other two parent domains of our model configuration on Lambert projection (ftp://aftp.fsl.noaa.gov/divisions/taq/global_emissions). The data are further processed, after the emissions are



mapped to all three domains, for compatibility with the gas-phase chemistry mechanism and the aerosol scheme of choice. Biogenic emissions are calculated (Guenther *et al.*, 1994) online through the USGS land-use classification and the WRF pre-processing system (WPS). Windblown dust emissions are calculated in the model using the US Air Force Weather Agency (AFWA) dust parameterization which includes the MB95 dust emission scheme (Marticorena and Bergametti, 1995) with typical airborne dust size distributions of Kok (2011).

The local emission inventory developed in this work is based on the total emission rates for each species derived from EDGAR for the whole domain. These total emission fluxes are spatially redistributed much more realistically based on the current land-use information for the state of Qatar. This is an important exercise for this region as the landscape of the metropolitan area of Doha has changed substantially over the last 10 years. Table 1 shows the WRF-Chem built-in 24-category USGS (United States Global Survey) land-use classification which, for the base case emissions is based on AVHRR (Advanced Very High Resolution Radiometer) satellite spanning April 1992 through March 1993 using a resolution of approximately 1 km. Accurate representation of land surface activity is relevant for an accurate estimation of emission rates and for appropriate modeling of the boundary layer evolution. Based on the current urban and build-up area coverage extracted from our GIS application in Qatar we recalculated anthropogenic emissions in high resolution (for each computational cell) while also updated all 24 categories coverage over our d03 domain. The global emissions have a resolution that varies from $50 \times 50 \text{ km}^2$ to $10 \times 10 \text{ km}^2$ resolution depending on the species and location in the EDGAR database. In our local emission inventory, our GIS exercise constructed emissions on a $0.2 \times 0.2 \text{ km}^2$ resolution, which were then mapped to our domain d03 that is resolved at $2 \times 2 \text{ km}^2$ resolution. For each computational cell of our domain, a percentage of each land use type is calculated from GIS information. The total (domain-wide) emission fluxes are then multiplied by a factor that represents the relevant land use type occupancy percentage to allocate emissions for this cell.

Fig. 2 shows the three most frequent categories in the land of Qatar with the original WRF land use input (AVHRR method) and the new land use information we constructed using GIS application.

Table 1. 24-category USGS land-use classification.

Category	Classification
1	Urban and Built-Up Land
2	Dryland Cropland and Pasture
3	Irrigated Cropland and Pasture
4	Mixed Dryland/Irrigated Cropland and Pasture
5	Cropland/Grassland Mosaic
6	Cropland/Woodland Mosaic
7	Grassland
8	Shrubland
9	Mixed Shrubland/Grassland
10	Savanna
11	Deciduous Broadleaf Forest
12	Deciduous Needleleaf Forest
13	Evergreen Broadleaf Forest
14	Evergreen Needleleaf Forest
15	Mixed Forest
16	Water Bodies
17	Herbaceous Wetland
18	Wooded Wetland
19	Barren or Sparsely Vegetated
20	Herbaceous Tundra
21	Wooded Tundra
22	Mixed Tundra
23	Bare Ground Tundra
24	Snow or Ice

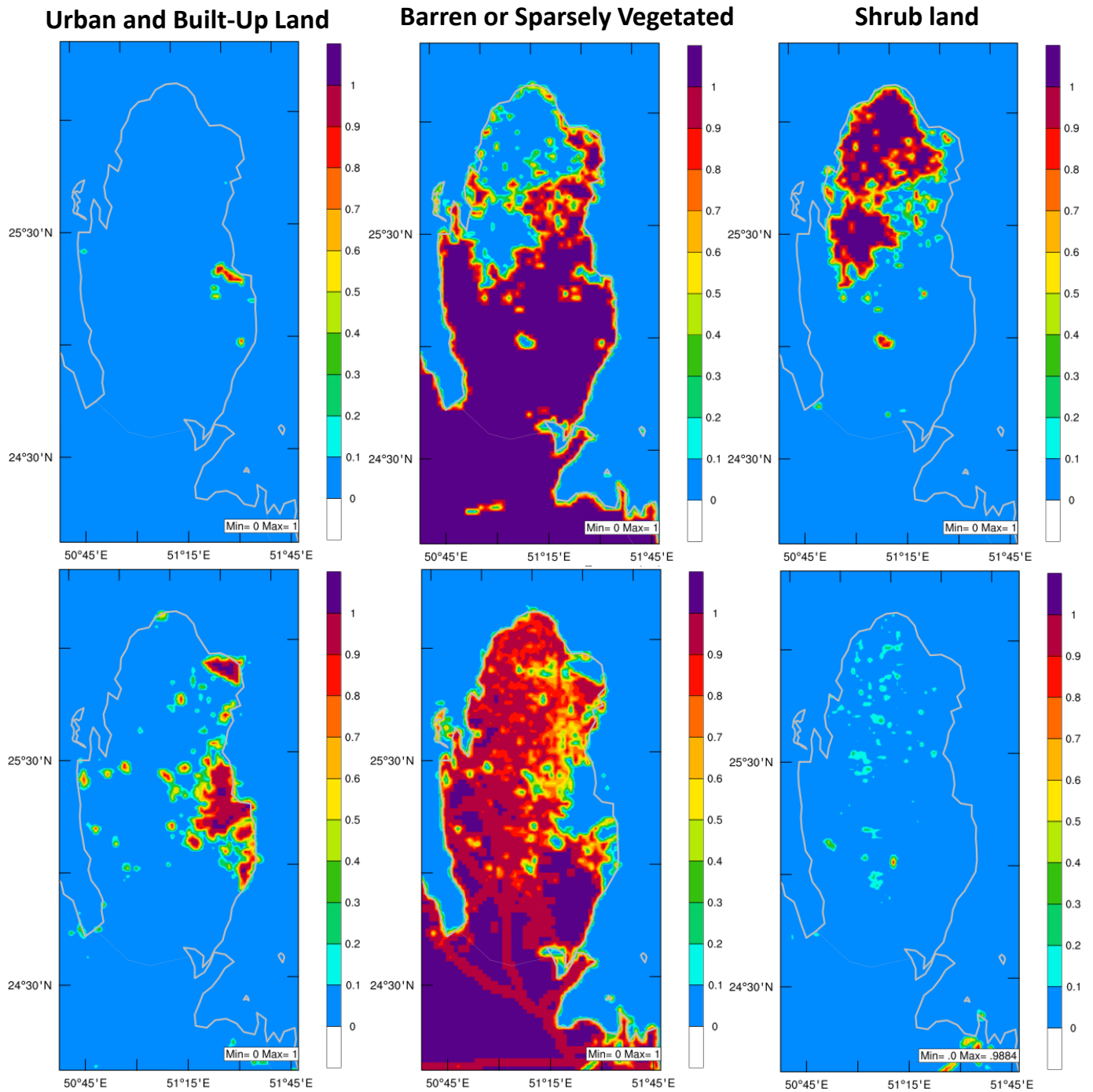
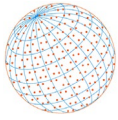


Fig. 2. Categories 1, 8 and 19 (from Table 1) representation in WRF land use input file using the default WRF method (top panels) and the newly constructed land use map based on recent GIS application (bottom panels). Scale is unitless (from 0–1, where 1 means 100% occupancy of the specific category in a computational cell).

Information from land category one (Classification: Urban and Build-up land) was used to redistribute the total anthropogenic emissions of Qatar. Furthermore, the WPS model, the pre-processor of WRF-Chem, was run with a new land use input file with all 24 categories updated.

2.3 Monitoring Data and Study Period

Surface observations were made by the Qatar Environment and Energy Research Institute (QEERI) which currently operates six Air quality Monitoring stations (AQMS) located in and outside the metropolitan area of Doha as shown in Fig. 3. All stations are equipped with: 1) a MP101M

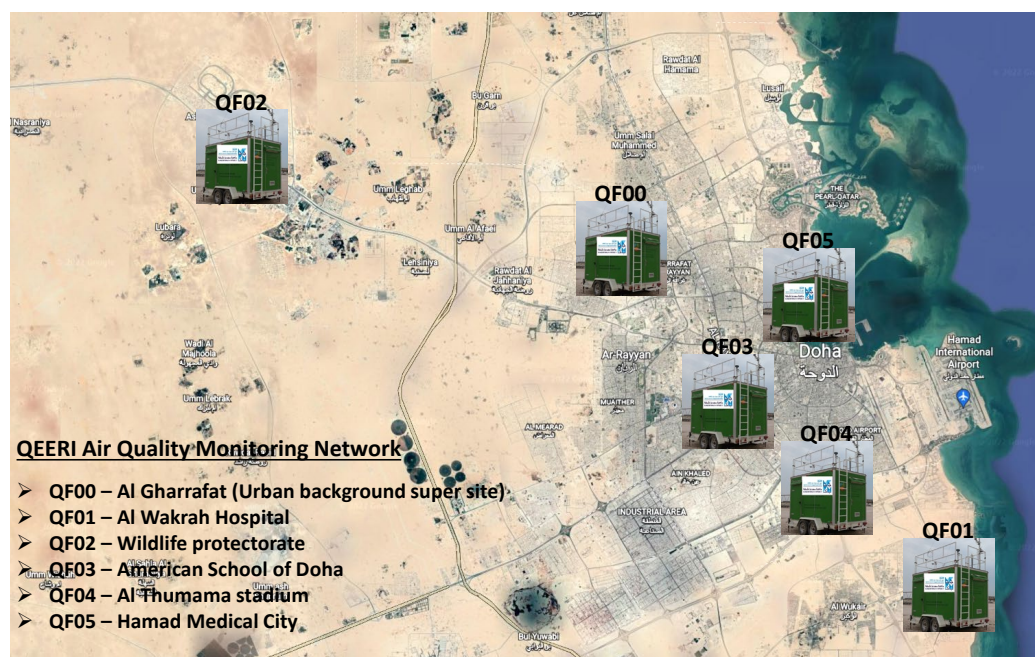
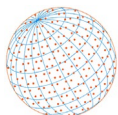


Fig. 3. Location of Air Quality Monitoring Stations in the greater metropolitan area of Doha, Qatar.

suspended particulate beta gauge monitor with continuous particulate measurement, 2) a AC32M chemiluminescent nitrogen oxide analyzer, 3) a AS32M optical Absorption Cavity attenuated phase-shift spectroscopy (CAPS), and 4) a O342 module UV photometric ozone analyzer. All AQMS are also equipped with Thermo-hygrometers (DMA867-875) for continuous measurements (every 1 min) of ambient relative humidity and temperature as well as Anemometers (DNA827) for the wind speed and wind direction. Following the standardized data validation methodology of the U.S. EPA (U.S. EPA, 2000), data quality assessment was performed routinely.

A full month of air quality forecasting was conducted for January 2021 using both the base case model configuration (EDGAR emissions) and the new version (high-resolution local emissions and land-use data).

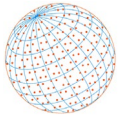
During this period, air quality and meteorological parameters were continuously monitored in 5 air quality measurement stations in Qatar (QF00-QF04; QF05 was not operational during the study period) and are used to assess the model's performance.

2.4 Model Verification

The model was run in operational forecasting mode, as detailed below. We produce forecasts of air quality, solar radiation and meteorology on hourly time resolution for 72 hours ahead for all three domains. A new forecast is run every day and initialized with the 00 UTC GFS global products of 27 km spatial resolution of NOAA (National Oceanic and Atmospheric Administration), NWS (National Weather Service), USA (<https://ftp.ncep.noaa.gov/data/nccf/com/gfs/prod/>). The forecasting skill of WRF-Chem/QEERI is quantified in terms of the root mean square error (RMSE), the mean gross error (MGE), the mean bias (MB), the FAC2 (fraction of predictions within a factor of two of the observation) and the forecast accuracy (FA; a perfect forecast would have FAC2 = 1 and FA = 100%):

$$RMSE = \sqrt{\frac{1}{N} \sum_{i=1}^n (P_i - O_i)^2} \quad (1)$$

$$MGE = \frac{1}{N} \sum_{i=1}^n |P_i - O_i| \quad (2)$$



$$MB = \frac{1}{N} \sum_{i=1}^n (P_i - O_i) \quad (3)$$

$$FAC2 = 0.5 \leq \frac{P_i}{O_i} \leq 2.0 \quad (4)$$

$$FA = \frac{\min(P_i, O_i)}{\max(P_i, O_i)} \times 100\% \quad (5)$$

where P_i is the model predicted value for data point i , O_i is the observed value and n is the total number of data points (hourly data). These are common statistics that have been widely used in similar studies around the world (Gonzales *et al.*, 2018; Kumar *et al.*, 2016; Hoshyaripour *et al.*, 2016). The first 12 hours of each simulation run are discarded as spin-up time.

3 RESULTS AND DISCUSSION

Fig. 4 shows nitrogen oxide (in $\text{mol km}^{-2} \text{hr}^{-1}$) and black carbon emissions (in $\mu\text{g m}^{-2} \text{hr}^{-1}$) from the base case simulation (i.e., EDGAR emission inventory) and by adopting our newly constructed local emission inventory using high resolution land-use information. The use of the up-to-date land-use scenario results in major differences in how topography is described within WRF-Chem, especially in terms of urban land cover, which in turn produces major differences in the magnitude and spatial distribution of emission rates. The footprint of the Doha metropolitan area on the anthropogenic NO and BC emissions is more realistically represented in the new version of emissions as seen in the east coast of Qatar in Fig. 4 (right panel).

We focus our model evaluation on O_3 , NO_x and $\text{PM}_{2.5}$ to analyze the impact of anthropogenic sources (e.g., vehicular and industrial) on anthropogenic air pollution in Doha. Furthermore, we present model skill statistics for the *air quality health index* (AQHI) calculated as described in Stieb *et al.* (2012) on an hourly frequency.

$$AQHI = \left(\frac{1000}{10.4} \right) \times \left[\left(e^{0.000537 \times \text{O}_3} - 1 \right) + \left(e^{0.000871 \times \text{NO}_2} - 1 \right) + \left(e^{0.000487 \times \text{PM}_{2.5}} - 1 \right) \right] \quad (6)$$

where O_3 and NO_2 are in parts per billion (ppb) while $\text{PM}_{2.5}$ in micrograms per cubic meter ($\mu\text{g m}^{-3}$). The AQHI provides a number from 1 to 10+ to indicate the level of health risk associated with local air quality. The index has been developed as a continuum: The higher the number, the greater the health risk and need to take precautions. The index describes the level of health risk associated with this number as 'low' (1–3; blue color), 'moderate' (4–6; orange color), 'high' (7–10; red color) or 'very high' (10+; purple color), and suggests steps that can be taken to reduce exposure. The formulation of WRF-Chem/QEERI's AQHI is based on the hourly forecast relationship of nitrogen dioxide, ground-level ozone and fine particulate matter as described in Eq. (6). These three pollutants are of concern in Doha, Qatar, based on long term observations from QEERI's network of AQ monitoring stations.

Table 2 shows the overall statistics for air quality parameters for both simulations. The simulation with the high resolution local emission inventory resulted in better model performance for all station locations in Qatar. Across all stations, the forecast accuracy increase from 28% to 76% for NO_x , from 60% to 87% for $\text{PM}_{2.5}$ and from 50% to 70% for AQHI. The most significant improvement was seen in the ASD station (QF03) located in the city center of Doha which is highly influenced by traffic pollution. The overall error dropped from –51% to 8% for $\text{PM}_{2.5}$ and from –88% to 20% for NO_x . The base case simulation significantly underpredicts concentrations of NO_x (Fig. 5) and $\text{PM}_{2.5}$ in the city which is mostly due to the different spatial allocation of local emissions. Urban anthropogenic pollution is much more realistically predicted in our new simulation runs adopting our newly constructed local emission inventory. The new emissions input resulted also in a much better prediction of the AQHI in all stations. The base case prediction of AQHI exhibited a mean

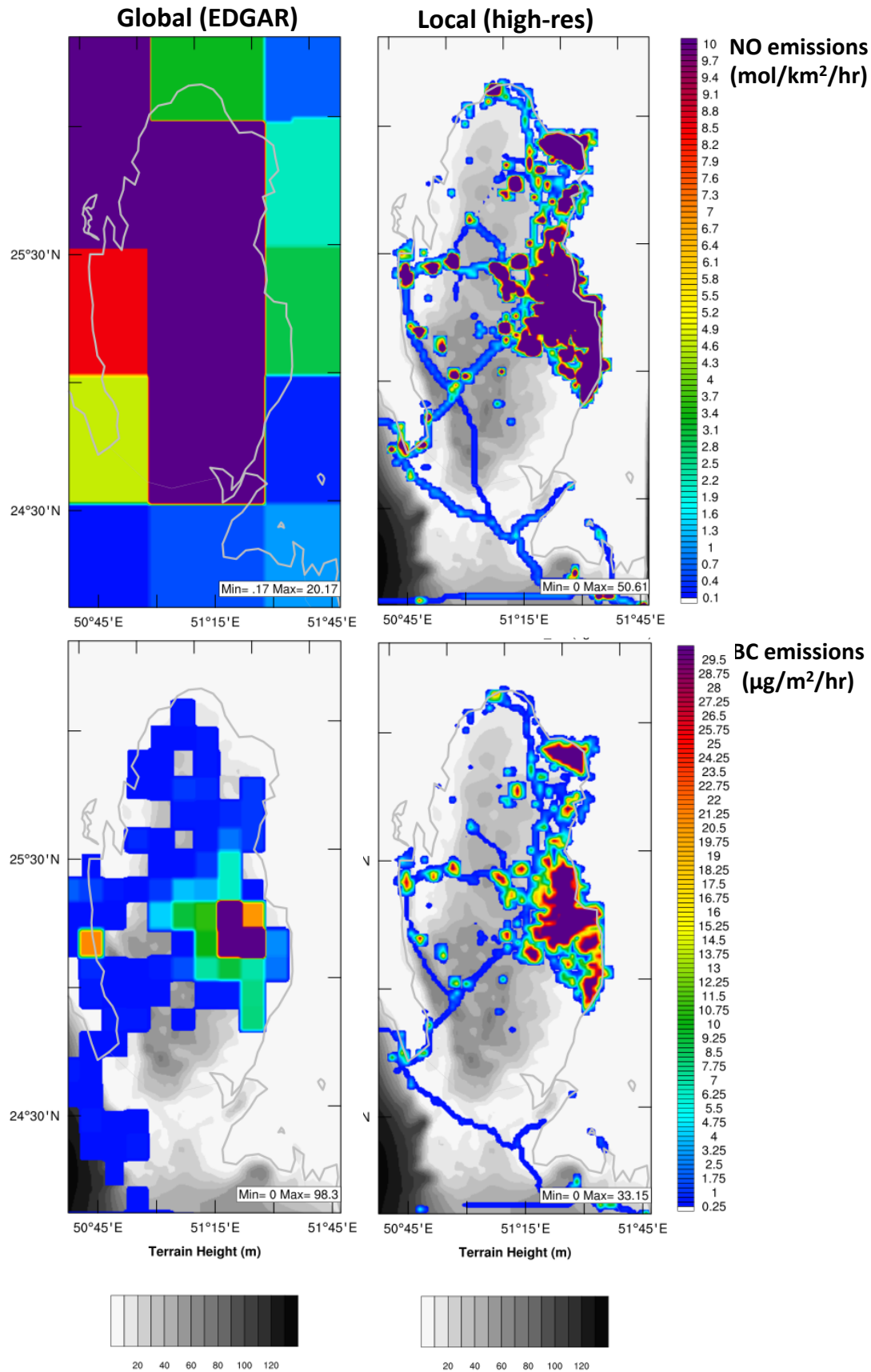
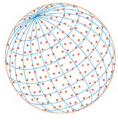


Fig. 4. WRF-Chem nitrogen oxide and black carbon emission rates in Qatar for the month of January 2021 estimated by the base case EDGAR emission inventory (left panels) and a local emission inventory based on current high-resolution land-use coverage data (right panels).

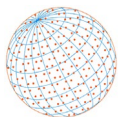


Table 2. Model performance statistics for five AQ monitoring stations in Qatar (the RMSE, MGE, and MB are given in $\mu\text{g m}^{-3}$ for $\text{PM}_{2.5}$ and in ppb for O_3 and NO_x).

Parameters	O_3	NO_x	$\text{PM}_{2.5}$	AQHI	O_3	NO_x	$\text{PM}_{2.5}$	AQHI
Statistics	Simulation				Simulation			
	Basecase (EDGAR emissions) at QF00				High-res (Local emissions) at QF00			
RMSE	15.49	46.25	33.80	3.33	12.18	37.12	36.79	2.60
MGE	12.30	26.46	26.42	2.80	9.44	21.40	23.10	1.96
MB	1.82	-26.07	-16.48	-2.64	1.70	3.95	-1.15	-1.36
FAC2 (%)	64.44	16.39	24.17	28.19	62.64	58.33	50.28	71.53
ME (%)	7.32	-77.29	-47.18	-52.29	6.84	11.70	-3.30	-26.89
	Basecase (EDGAR emissions) at QF01				High-res (Local emissions) at QF01			
RMSE	17.84	67.70	18.15	2.55	13.93	57.41	22.08	2.10
MGE	13.95	44.10	12.17	2.07	10.78	34.13	14.36	1.56
MB	5.05	-44.05	-4.51	-2.00	4.81	-25.19	4.44	-1.27
FAC2 (%)	51.11	4.03	29.03	28.89	51.81	28.75	36.11	57.50
ME (%)	24.10	-92.26	-29.40	-51.91	22.98	-52.76	28.96	-32.92
	Basecase (EDGAR emissions) at QF02				High-res (Local emissions) at QF02			
RMSE	16.53	21.61	32.61	2.17	13.11	21.37	34.78	2.13
MGE	12.85	11.02	23.53	1.71	10.19	13.23	24.73	1.56
MB	-2.59	-4.91	-11.64	-1.42	-2.67	2.53	-5.81	-1.00
FAC2 (%)	63.47	39.31	32.08	58.75	60.83	41.81	36.67	62.08
ME (%)	-9.29	-32.69	-35.16	-35.98	-8.79	14.71	-20.28	-26.69
	Basecase (EDGAR emissions) at QF03				High-res (Local emissions) at QF03			
RMSE	15.67	70.17	25.27	3.55	12.31	55.43	23.69	2.41
MGE	12.26	43.29	18.49	3.06	9.15	28.98	16.15	1.93
MB	3.06	-43.27	-13.17	-3.02	4.21	-9.98	2.17	-1.62
FAC2 (%)	56.11	5.00	26.25	21.53	57.22	53.89	50.14	73.06
ME (%)	14.11	-88.14	-51.77	-60.49	19.41	-20.33	8.54	-33.73
	Basecase (EDGAR emissions) at QF04				High-res (Local emissions) at QF04			
RMSE	17.44	138.16	34.06	4.53	14.89	122.08	27.38	3.48
MGE	13.60	89.68	26.78	3.82	11.66	69.79	20.12	2.74
MB	5.61	-89.68	-23.37	-3.80	5.61	-61.00	-9.45	-2.61
FAC2 (%)	56.94	1.25	14.44	11.67	54.31	33.89	43.89	47.50
ME (%)	26.06	-95.75	-67.15	-66.52	26.05	-65.20	-27.15	-45.65

bias ranging from -1.4 (in the desert) to -3 (in the city center) which highly improved in our new model version (from -1 to -1.6).

In the background location of the Shahaniya station (QF02), which is close to Qatar's desert, there is a significant improvement in the predictions of all air quality parameters which shows the influence of the city's pollution to the greater region in Qatar. The improvement in ozone concentration predictions appears small on average (Table 2) since ozone is a secondary pollutant and more regionally distributed regardless of the emission inventory used. However, significant differences occurred in the diurnal profile of ozone. Fig. 6 shows the temporal variation of ozone concentrations from the two different forecasts (i.e., with EDGAR and with our new local emission inventory) along with NO_x concentrations against the observed data at our supersite location, QF00 station, which is characterized as an urban background site of Doha.

The use of local emissions systematically helps the forecast capture the diurnal variation of ozone much better than the forecast with the global (EDGAR) emissions for Doha. A substantial improvement of the spatial allocation of ozone precursors (NO_x and *NMVOCS*) together with the higher resolution allowed for better representation of the formation of diurnal profiles of ozone production and titration. The daily maximum values are well represented in the new simulation; this is important for the development of effective mitigation strategies and AQ management plans at urban environments. Night-time observed minimum ozone concentrations are often overpredicted even with the new emissions indicating that further improvements are needed

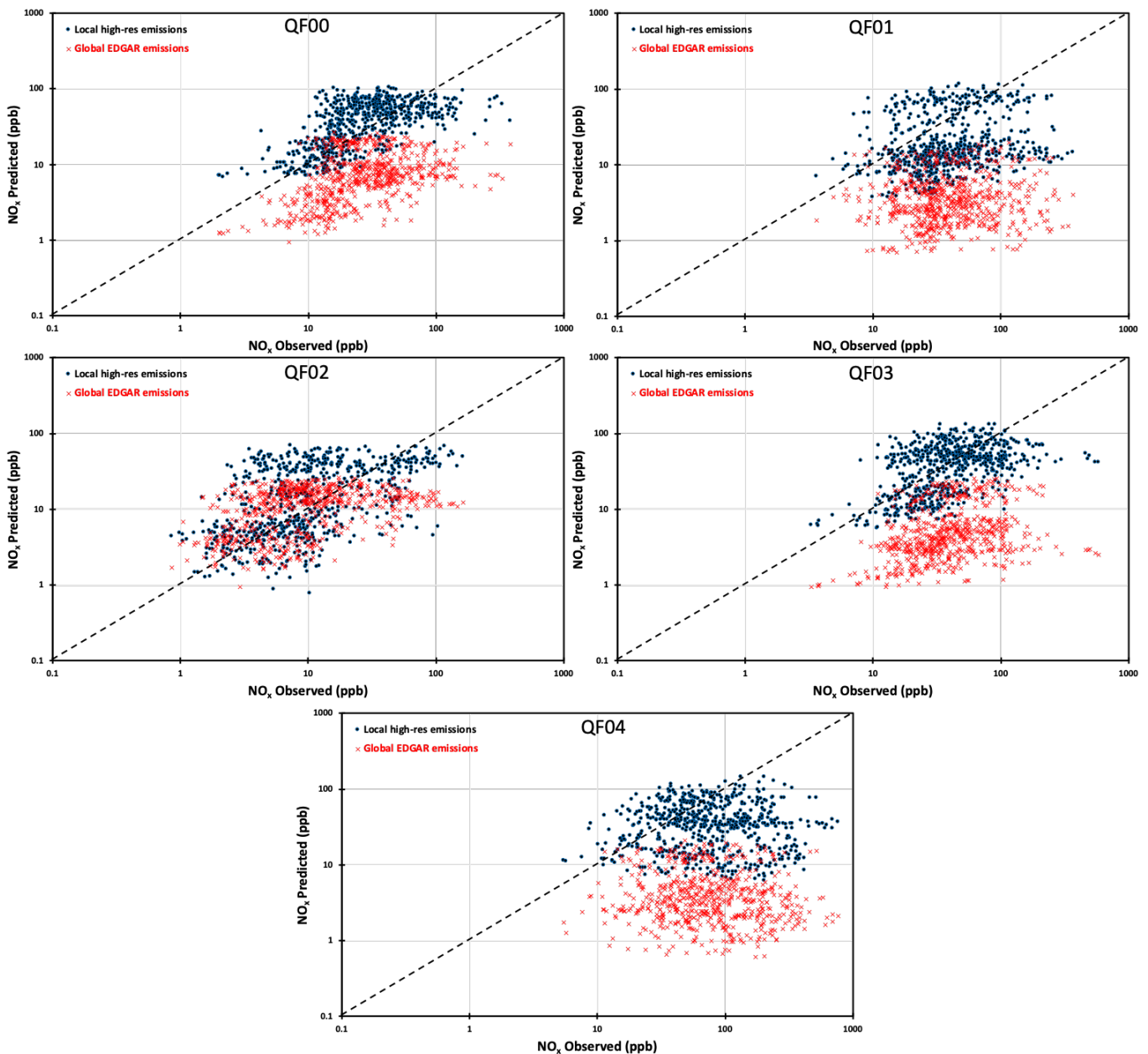
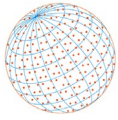


Fig. 5. Scatter plot comparison of observed and predicted hourly NO_x in five monitoring stations in Qatar (QF00–QF04 as shown in Fig. 2) using the global EDGAR and local high-resolution emissions.

possibly in the NO_x and VOC_s emission profiles. Also, hyperlocal sources of anthropogenic emissions (e.g., construction machinery emissions) missing from our inventory are also a source of forecast error. This is particularly the case with the location of the QF04 AQMS. A significant improvement in the time series forecast is also seen for NO_x concentrations, not so much towards the diurnal capture as with the O_3 case, but rather in the magnitude of the NO_x levels throughout the day. Fig. 7 shows the average spatial distribution of $\text{PM}_{2.5}$ and NO_x concentrations in Qatar for January 2021 predicted by the two simulations. Significant differences in both the quantity and allocation of primary anthropogenic emission inputs between the two inventories used, resulted in locally significant differences in spatial distribution of $\text{PM}_{2.5}$ and NO_x concentrations. Results show that the local (high-res) simulation forecasts increased the levels of $\text{PM}_{2.5}$ over the mainland of Qatar, where the atmospheric particle composition is rich in suspended dust particles. $\text{PM}_{2.5}$ and NO_x concentrations also increased over the metropolitan area of Doha, the industrial cities of Ras-Laffan in the north, and Mesaieed in the Southeast of Doha. On the contrary, the base case simulation

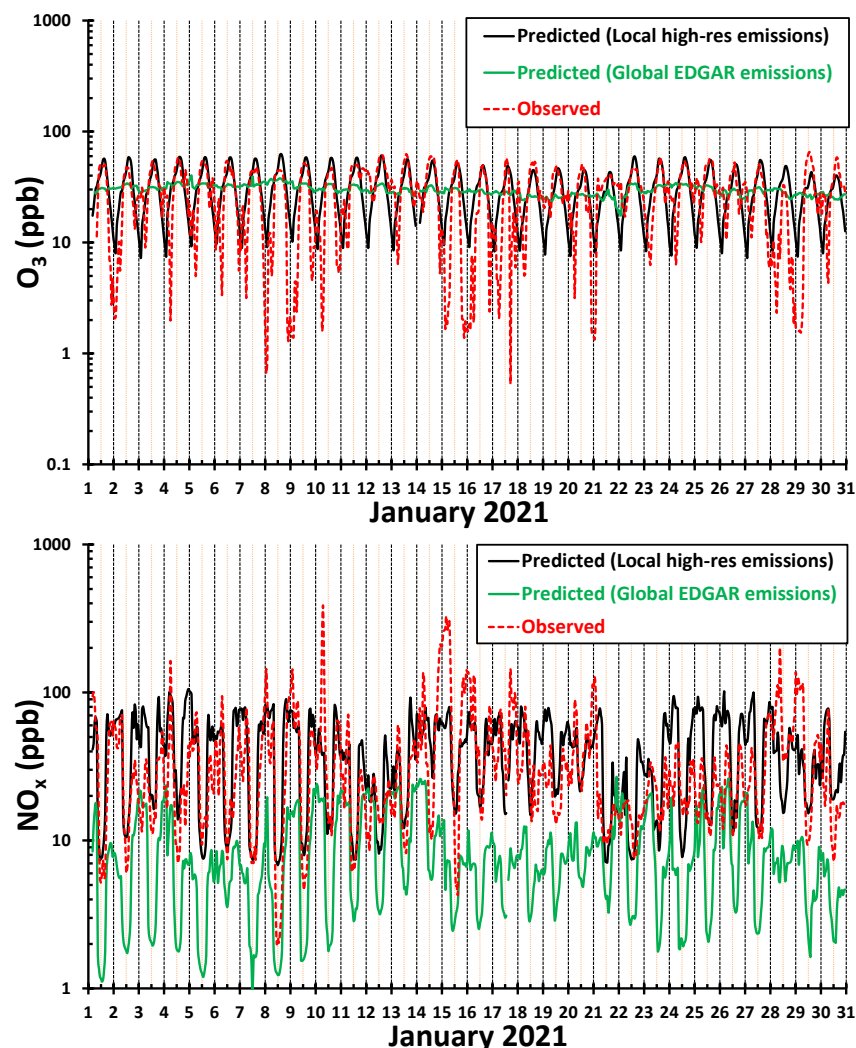
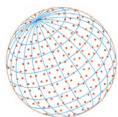


Fig. 6. Timeseries comparison of observed and predicted hourly O_3 (top panel) and NO_x (bottom panel) in our urban background station in Qatar (QF00) using the global EDGAR and local high-resolution emissions.

shows elevated $PM_{2.5}$ only over the desert of Qatar. Model performance statistics for the QF00 AQMS, which is our urban background station, clearly shows the forecast skill improvement when using the high-res local emission inventory. The overall $PM_{2.5}$ mean error at QF00 decreased from -47% to -3% while the mean bias from $-16 \mu g m^{-3}$ to $-1 \mu g m^{-3}$. The forecast accuracy for NO_x improved from 48% to 73%. It should be noted that the overall model performance regarding meteorological parameters was very encouraging while the two simulations did not produce significant differences. Overall, the error for temperature ranged between 2 and 5% among stations, 10–12% for relative humidity while the MGE for winds ranged between 0.9 and $1.2 m s^{-1}$ without any systematic bias. The use of the new high-res emission inventory significantly improves the representation of the AQHI across Qatar (Table 3), with the only exception of the Al Thumama station: this is due to the presence of a local construction site that was not accounted for in our local inventory. The base case version, which adopts the EDGAR inventory, systematically underpredicted the AQHI values in all AQMS locations.

4 CONCLUSIONS

In this study we apply the 3-D regional chemical transport model WRF-Chem over the Middle East with a high grid resolution over the Arabian Peninsula and the state of Qatar during January

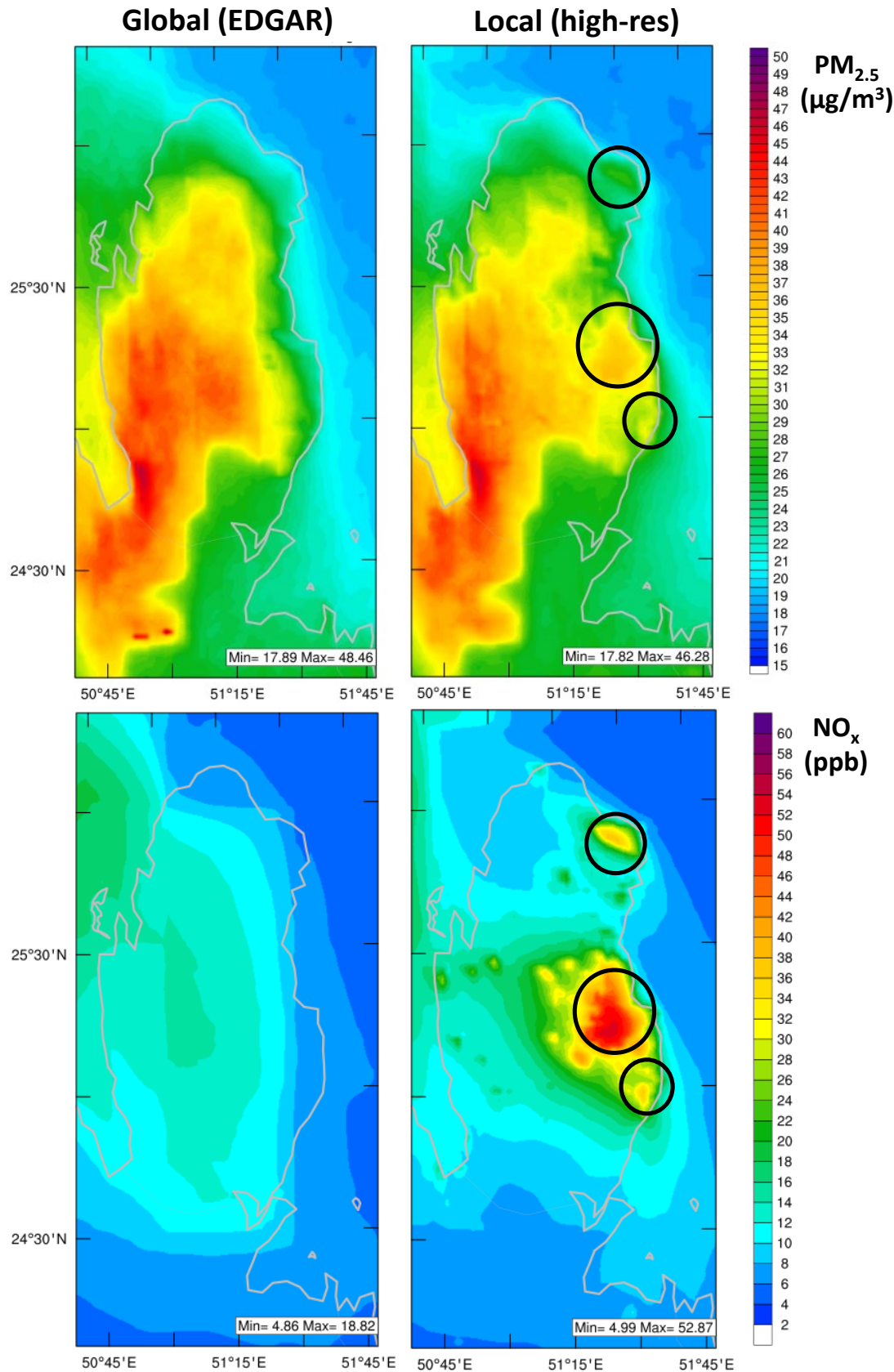
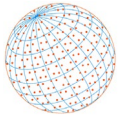


Fig. 7. WRF-Chem PM_{2.5} (top panels) and NO_x concentrations (bottom panels) in Qatar for the month of January 2021 predicted by the base case forecast simulation [using EDGAR emission inventory (left panels)] and the new forecast simulation [using a local emission inventory based on current high-resolution land-use coverage data (right panels)]. Black circles show the location of the metropolitan area of Doha, and the industrial cities of Ras-Laffan in the north and Mesaieed in the Southeast of Doha.

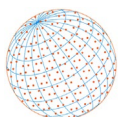


Table 3. Comparison of monthly averaged (January 2021) observed AQHI in five monitoring stations in Qatar against the WRF-Chem/QEERI forecast using the global EDGAR and local high-resolution emissions.

AQHI	Observed	Forecast Basecase	Forecast High-res
QF00	MODERATE	LOW	MODERATE
QF01	MODERATE	LOW	MODERATE
QF02	MODERATE	LOW	MODERATE
QF03	MODERATE	LOW	MODERATE
QF04	HIGH	LOW	MODERATE

2021 in operational forecasting mode. We test the sensitivity of the predictions of PM_{2.5}, Ozone and NO_x on the anthropogenic emission inventory used over Qatar. The forecast accuracy is evaluated against surface observations taken from five Air quality Monitoring stations located in and outside the metropolitan area of Doha, Qatar. A local emission inventory is developed based on the total EDGAR emission rates that are re-distributed over Qatar in a more realistic way using updated land-use information in high spatial resolution. The global emissions have a resolution that varies from 50 × 50 km² to 10 × 10 km² resolution over Qatar depending on the species and location in the EDGAR database. In our local emission inventory, GIS is applied to construct emissions on a 0.2 × 0.2 km² resolution, which were then mapped to our WRF-Chem domain in Qatar at 2 × 2 km² resolution. A significant improvement in the forecast accuracy was found when employing the new inventory. The overall error across all stations was reduced from -51% to 8% for PM_{2.5} and from -88% to 20% for NO_x, while a significant improvement was observed in the diurnal profile of predicted ozone. Moreover, the new inventory resulted in a more accurate forecast of the air quality health index. Across all stations, the forecast accuracy increase from 28% to 76% for NO_x, from 60% to 87% for PM_{2.5} and from 50% to 70% for AQHI. Future applications of WRF-Chem with EDGAR emissions over the Middle East could benefit a lot from employing our methodology for a much more accurate re-construction of the anthropogenic emission inventory.

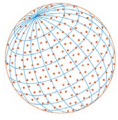
ACKNOWLEDGMENTS

The authors acknowledge the use of Qatar Environment and Energy Research Institute (QEERI) HPC (High Performance Computer cluster) resources.

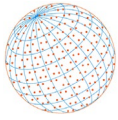
The publication of this article was funded by Qatar National Library.

REFERENCES

- Anisimov, A., Tao, W., Stenchikov, G., Kalenderski, S., Prakash, P.J., Yang, Z.L., Shi, M. (2017). Quantifying local-scale dust emission from the Arabian Red Sea coastal plain. *Atmos. Chem. Phys.* 17, 993–1015. <https://doi.org/10.5194/acp-17-993-2017>
- Bel, G., Joseph, S. (2015). Emission abatement: Untangling the impacts of the EU ETS and the economic crisis. *Energy Econ.* 49, 531–539. <https://doi.org/10.1016/J.ENERCO.2015.03.014>
- Chen, S.H., Sun, W.Y. (2002). A one-dimensional time dependent cloud model. *J. Meteorol. Soc. Jpn.* 80, 99–118, <https://doi.org/10.2151/jmsj.80.99>
- Fast, J.D., Gustafson, W.I.Jr., Easter, R.C., Zaveri, R.A., Barnard, J.C., Chapman, E.G., Grell, G.A. (2006). Evolution of ozone, particulates, and aerosol direct forcing in an urban area using a new fully coupled meteorology, chemistry, and aerosol model. *J. Geophys. Res.* 111, D21305. <https://doi.org/10.1029/2005JD006721>
- Font, A., Fuller, G.W. (2016). Did policies to abate atmospheric emissions from traffic have a positive effect in London? *Environ. Pollut.* 218, 463–474. <https://doi.org/10.1016/j.envpol.2016.07.026>
- Fountoukis, C., Ackermann, L., Ayoub, M.A., Gladich, I., Hoehn, R.D., Skillern, A. (2016). Impact of



- atmospheric dust emission schemes on dust production and concentration over the Arabian Peninsula. *Model. Earth Syst. Environ.* 2, 115. <https://doi.org/10.1007/s40808-016-0181-z>
- Fountoukis, C., Ayoub, M.A., Ackermann, L., Perez-Astudillo, D., Bachour, D., Gladich, I., Hoehn, R.D. (2018). Vertical ozone concentration profiles in the Arabian Gulf region during summer and winter: Sensitivity of WRF-Chem to planetary boundary layer schemes. *Aerosol Air Qual. Res.* 18, 1183–1197. <https://doi.org/10.4209/aaqr.2017.06.0194>
- Fountoukis, C., Harshvardhan, H., Gladich, I., Ackermann, L., Ayoub, M.A. (2020). Anatomy of a severe dust storm in the Middle East: Impacts on aerosol optical properties and radiation budget. *Aerosol Air Qual. Res.* 20, 155–165. <https://doi.org/10.4209/aaqr.2019.04.0165>
- Geiger, H., Barnes, I., Bejan, I., Benter, T., Spittler, M. (2003). The tropospheric degradation of isoprene: An updated module for the regional atmospheric chemistry mechanism. *Atmos. Environ.* 37, 1503–1519. [https://doi.org/10.1016/S1352-2310\(02\)01047-6](https://doi.org/10.1016/S1352-2310(02)01047-6)
- Ginoux, P., Chin, M., Tegen, I., Prospero, J.M., Holben, B., Dubovik, O., Lin, S.J. (2001). Sources and distributions of dust aerosols simulated with the GOCART model. *J. Geophys. Res.* 106, 20255–20273. <https://doi.org/10.1029/2000JD000053>
- González, C.M., Ynoue, R.Y., Vara-Vela, A., Rojas, N.Y., Aristizábal, B.H. (2018). High-resolution air quality modeling in a medium-sized city in the tropical Andes: Assessment of local and global emissions in understanding ozone and PM₁₀ dynamics. *Atmos. Pollut. Res.* 9, 934–948. <https://doi.org/10.1016/j.apr.2018.03.003>
- Grell, G.A., Dévényi, D. (2002). A generalized approach to parameterizing convection combining ensemble and data assimilation techniques. *Geophys. Res. Lett.* 29, 38-1–38-4. <https://doi.org/10.1029/2002GL015311>
- Grell, G.A., Peckham, S.E., Schmitz, R., McKeen, S.A., Frost, G., Skamarock, W.C., Eder, B. (2005). Fully coupled “online” chemistry within the WRF model. *Atmos. Environ.* 39, 6957–6975. <https://doi.org/10.1016/j.atmosenv.2005.04.027>
- Guenther, A., Zimmerman, P., Wildermuth, M. (1994). Natural volatile organic compound emission rate estimates for US woodland landscapes. *Atmos. Environ.* 28, 1197–1210. [https://doi.org/10.1016/1352-2310\(94\)90297-6](https://doi.org/10.1016/1352-2310(94)90297-6)
- Hoesly, R.M., Smith, S.J., Feng, L., Klimont, Z., Janssens-Maenhout, G., Pitkanen, T., Seibert, J.J., Vu, L., Andres, R.J., Bolt, R.M., Bond, T.C., Dawidowski, L., Kholod, N., Kurokawa, J., Li, M., Liu, L., Lu, Z., Moura, M.C.P., O'Rourke, P.R., Zhang, Q. (2018). Historical (1750–2014) anthropogenic emissions of reactive gases and aerosols from the Community Emissions Data System (CEDS). *Geosci. Model Dev.* 11, 369–408. <https://doi.org/10.5194/gmd-11-369-2018>
- Hong, S.Y., Noh, Y., Dudhia, J. (2006). A new vertical diffusion package with an explicit treatment of entrainment processes. *Mon. Weather Rev.* 134, 2318–2341. <https://doi.org/10.1175/MWR3199.1>
- Hoshyaripour, G., Brasseur, G., Andrade, M.F., Gavidia-Calderón, M., Bouarar, I., Ynoue, R.Y. (2016). Prediction of ground-level ozone concentration in São Paulo, Brazil: deterministic versus statistic models. *Atmos. Environ.* 145, 365–375. <https://doi.org/10.1016/j.atmosenv.2016.09.061>
- Jish Prakash, P., Stenchikov, G., Kalenderski, S., Osipov, S., Bangalath, H. (2015). The impact of dust storms on the Arabian Peninsula and the Red Sea. *Atmos. Chem. Phys.* 15, 199–222. <https://doi.org/10.5194/acp-15-199-2015>
- Kalenderski, S., Stenchikov, G., Zhao, C. (2013). Modeling a typical winter-time dust event over the Arabian Peninsula and the Red Sea. *Atmos. Chem. Phys.* 13, 1999–2014. <https://doi.org/10.5194/acp-13-1999-2013>
- Karagulian, F., Temimi, M., Ghebreyesus, D., Weston, M., Kondapalli, N.K., Valappil, V.K., Aldababesh, A., Lyapustin, A., Chaouch, N., Al Hammadi, F., Al Abdooli, A. (2019). Analysis of a severe dust storm and its impact on air quality conditions using WRF-Chem modeling, satellite imagery, and ground observations. *Air Qual. Atmos. Health* 12, 453–470. <https://doi.org/10.1007/s11869-019-00674-z>
- Kok, J.F. (2011). A scaling theory for the size distribution of emitted dust aerosols suggests climate models underestimate the size of the global dust cycle. *PNAS* 108, 1016–1021. <https://doi.org/10.1073/pnas.1014798108>
- Kontos, S., Liora, N., Giannaros, C., Kakosimos, K., Poupkou, A., Melas, D. (2018). Modeling natural dust emissions in the central Middle East: Parameterizations and sensitivity. *Atmos. Environ.* 190, 294–307. <https://doi.org/10.1016/j.atmosenv.2018.07.033>



- Kumar, A., Jiménez, R., Belalcázar, L.C., Rojas, N.Y. (2016). Application of WRF-chem model to simulate PM₁₀ concentration over Bogotá. *Aerosol Air. Qual. Res.* 16, 1206–1221. <https://doi.org/10.4209/aaqr.2015.05.0318>
- Longo, K.M., Freitas, S.R., Pirre, M., Marécal, V., Rodrigues, L.F., Panetta, J., Alonso, M.F., Rosário, N.E., Moreira, D.S., Gácita, M.S., Arteta, J., Fonseca, R., Stockler, R., Katsurayama, D.M., Fazenda, A., Bela, M. (2013). The Chemistry CATT-BRAMS model (CCATT-BRAMS 4.5): A regional atmospheric model system for integrated air quality and weather forecasting and research. *Geosci. Model Dev.* 6, 1389–1405. <https://doi.org/10.5194/gmd-6-1389-2013>
- Marticorena, B., Bergametti, G. (1995). Modeling the atmospheric dust cycle. 1. Design of a soil-derived dust emission scheme. *J. Geophys. Res.* 100, 16415–16430. <https://doi.org/10.1029/95JD00690>
- Mlawer, E.J., Taubman, S.J., Brown, P.D., Iacono, M.J., Clough, S.A. (1997). Radiative transfer for inhomogeneous atmospheres: RRTM, a validated correlated-k model for the longwave. *J. Geophys. Res.* 102, 16663–16682. <https://doi.org/10.1029/97JD00237>
- Parajuli, S.P., Stenchikov, G.L., Ukhov, A., Kim, H. (2019). Dust emission modeling using a new high-resolution dust source function in WRF-Chem with implications for air quality. *J. Geophys. Res.* 124, 10109–10133. <https://doi.org/10.1029/2019JD030248>
- Roshan, D., Koc, M., Isaifan, R., Shahid, M.Z., Fountoukis, C. (2019). Aerosol optical thickness over large urban environments of the Arabian Peninsula—Speciation, variability, and distributions. *Atmosphere* 10, 228. <https://doi.org/10.3390/atmos10050228>
- Stieb, D.M., Burnett, R.T., Smith-Doiron, M., Brion, O., Shin, H.H., Economou, V. (2012). A new multipollutant, no-threshold air quality health index based on short-term associations observed in daily time-series analyses. *J. Air Waste Manage. Assoc.* 58, 435–450. <https://doi.org/10.3155/1047-3289.58.3.435>
- Stockwell, W.R., Kirchner, F., Kuhn, M., Seefeld, S. (1997). A new mechanism for regional atmospheric chemistry modeling. *J. Geophys. Res.* 102, 25847–25879. <https://doi.org/10.1029/97JD00849>
- Ukhov, A., Mostamandi, S., da Silva, A., Flemming, J., Alshehri, Y., Shevchenko, I., Stenchikov, G. (2020). Assessment of natural and anthropogenic aerosol air pollution in the Middle East using MERRA-2, CAMS data assimilation products, and high-resolution WRF-Chem model simulations. *Atmos. Chem. Phys.* 20, 9281–9310. <https://doi.org/10.5194/acp-20-9281-2020>